PROCEEDINGS, 43rd Workshop on Geothermal Reservoir Engineering
Stanford University, Stanford, California, February 12-14, 2018
SGP-TR-213

Mechanical Responses of Formation and Wellbore Induced by Water Injection for Enhanced Geothermal System

Fei Yin [1,2], Lihong Han [3], Shangyu Yang [3], Ziyi Xu [2,*], Yang Xiao [1], Xingru Wu [2]

[1] College of Energy, Chengdu University of Technology, Chengdu, Sichuan 610059, China

[2] The Mewbourne School of Petroleum & Geological Engineering, The University of Oklahoma, Norman, OK 73019, USA

[3] Tubular Goods Research Institute of CNPC, Xi'an, Shanxi 710000, China

* Corresponding author.

ziyi.xu@ou.edu (Z. Xu); yinfei@ou.edu (F. Yin).

Keywords: geothermal development; THM model; formation response; well integrity

ABSTRACT

Water injection is often needed for enhanced geothermal system (EGS) as the primary thermal recovery is low for many geothermal reservoirs. Water injection causes the variations of temperature, pore pressure and in-situ stress in the swept region. It also could cause wellbore deformation and compromise the wellbore integrity. In this paper, a thermo-hydro-mechanical (THM) fully-coupled model of formation and wellbore is established. The formation is simplified as a poroelastic medium. The casing and cement sheath in injection and production wells are embedded in the formation. The THM responses of formation and the mechanical behavior of wellbore are simulated synchronously in EGS. Results indicate that the pore pressure decreases from injection well to production well and the water temperature rises during flowing into production well. A low-temperature region (LTR) forms around the injection well and expands as the operation continues. Temperature propagates much slower than overpressure. The effective stress decreases around the injection well due to overpressure and thermal contraction. Overpressure and thermal contraction causes a fluctuant deformation of formation. The thermal effect overwhelms the poroelastic effect in the late period. The Mises stress of the casing in injection well reaches to its maximum value soon and then decreases slightly. While, the Mises stress of the casing in production well increases gradually after thermal breakthrough. This research provides a reference for evaluating formation THM response and wellbore integrity in geothermal development.

1. INTRODUCTION

As one of the promising and clean renewable energy resources, geothermal resources have been used for electricity generation, heating and cooling in many countries, including USA, Iceland, New Zealand and Indonesia (Pandey et al., 2017; Wang et al., 2017). In the enhanced geothermal system (EGS), the geothermal energy is extracted by injecting fluid through fractures (Rawal, 2012; Ye et al., 2017). Fluid injection in EGS causes the variations of pore pressure, temperature and stress/deformation because of the poroelastic and thermoelastic effects. It influences the hydraulic and thermal performances and potentially compromises the wellbore integrity.

Analyzing the coupled thermo-hydro-mechanical (THM) interaction is the key to understand the response of geothermal reservoir under injection. Ge and Ghassemi (2008) studied the impact of the in-situ stress, pore pressure, poroelastic and thermoelastic phenomena on the rock failure around a hydraulic fracture. Simone et al. (2013) investigated THM effect of cold water injection in a porous fractured formation and found that rock instability was the superposition of hydraulic and thermal effects. Huang (2014) coupled the reservoir-wellbore simulators and predicted the desirable thermal efficiency in Songliao Basin although a significant decrease in production due to thermal depletion. Kim and Hosseini (2015) simulated the THM effects by using the COMSOL software. Li et al. (2016) analyzed the microscopic behavior of THM mechanisms by discrete element method (DEM), and found that thermal stress can greatly enhance initiation and propagation of fractures. Cooling and overpressure resulted in the decrease of effective stress and increase of fracture aperture (Zhao et al., 2015). Additionally, the porosity in most zone increases resulting from injection and temperature drop (Huang et al., 2016; Simone et al., 2013). The heat flow within the fracture is convection dominated; while heat transfer in other impermeable zones is conduction dominated (Mossap, 2001). Moreover, hot water extraction can cause formation deformation in the case of excessive pressure depletion, which can compromise the existing infrastructures (Samsonov et al., 2011; Sarychikhina and Glowacka, 2015). For example, the surface deformation measured with InSAR was −10~25 mm in the In Salah storage site (White et al., 2014). The THM interaction in reservoir affects the caprock stability (Li, 2017) and well integrity.

Surveyed literature has little discussion on fluid injection impact on wellbore, especially casing, responses. In this study, an integrated THM coupled model consisting of reservoir/layers, injection/production wells and casings, is proposed to predict the mechanical behavior of casings in injection and production wells.

2. MODELING

2.1 Coupled Equations

When formation undergoes the variations of pore pressure and temperature, a system of equations, which is governing fluid flow in porous media, thermal energy balance, and deformation in the formation must be solved to accurately predict the geothermal reservoir behavior.

Figure 1 shows the coupled relationships among temperature, seepage and deformation considered in the THM model. Note that the cooling effect of injection induces the decrease of thermal stress and the contraction of rock skeleton.

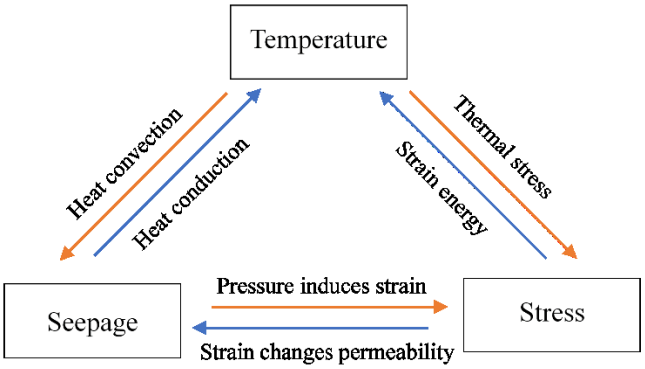

Figure 1: Coupling mechanics of thermos-poroelastic process.

The following assumptions are made to simplify the THM model (Safari and Ghassemi, 2015):

- The geothermal reservoir is homogeneous and isotropic on porous and permeability.
- The geothermal reservoir is saturated with a single-phase fluid.
- Linear heat conduction governs heat transfer.
- The material parameters are constant.

Thermo-poroelasticity is based on Biot's poroelasticity generalized to account for the temperature change. It coupled the fluid flow, temperature field and rock deformation. The governing equations for THM model have been derived by Aboustit et al. (1985) and Lewis et al. (1986). The Navier-type equilibrium equation in porous media can be written as:

$$Gu_{i,ij} + (\lambda + G)u_{j,ji} = \alpha_B p_{,i} + K_V \alpha_{Ts} T_{,i} - f_i \tag{1}$$

Where u is displacement vector, p is pore pressure, T is temperature, λ, G are Lame constant, α_B is the Biot coefficient, α_{Ts} is the thermal expansion coefficient of rock skeleton, f_i is body force vector, $K_V = E/[3(1-2\nu)]$ is the body deformation modulus, E is Young's modulus, ν is Poisson's ratio.

Substituting the Darcy's law into the continuity equation, the flow in porous medium is expressed as:

$$-\nabla^T \left[\frac{\mathbf{k}}{\mu} \nabla (p + \rho_w g z) \right] + \alpha_B \mathbf{m}^T \frac{\partial \varepsilon}{\partial t} - \left[\phi \alpha_{Tw} + (1-\phi)\alpha_{Ts} \right] \frac{\partial T}{\partial t} = Q_m \tag{2}$$

Where $\mathbf{k}$ is the matrix of permeability, $\mathbf{m}^T = [1\ 1\ 1\ 0\ 0\ 0]$, ρ_w is the water density, μ is the water viscosity, ε is the volume strain, ϕ is the porosity, α_{Tw} is thermal expansion coefficient of water, Q_m is the source term.

Inserting Fourier's law into the energy balance equation and adding the items of the heat convection and strain energy (Tao et al., 2013), the heat diffusion equation is obtained as:

$$-\nabla^T k_{heq} \nabla T + (\rho C)_{eq} \frac{\partial T}{\partial t} + \rho_w C_w \mathbf{V}_w^T \nabla T + (1-\phi) T K_V \alpha_{Ts} \mathbf{m}^T \frac{\partial \boldsymbol{\varepsilon}}{\partial t} = Q_h \tag{3}$$

Where $k_{heq} = k_{hw}\phi + k_{hs}(1-\phi)$ is the equivalent thermal conductivity coefficient, k_{hw} is thermal conductivity coefficient of water, k_{hs} is thermal conductivity coefficient of skeleton, $(\rho C)_{eq} = \rho_w C_w \phi + \rho_s C_s (1-\phi)$ is the volumetric heat capacity, ρ_s is the density of skeleton, C_w is the specific heat of water, C_s is the specific heat of skeleton, V_w is the flow velocity, Q_h is the heat flux.

For given boundary/initial conditions, these equations can be solved numerically. Computation iterates among the equations at each time step using a finite element method (Kim and Hosseini, 2015).

2.2 Numerical Modeling

Figure 2 shows the diagram of a typical EGS with injectors and producers. Cold water is injected into the geothermal reservoir, and hot water is being extracted from the producers. The reservoir, the study objective in mathematic model, is bounded by the caprock and underlayer. The fracture-matrix system of the fractured reservoir caused by hydraulic fracturing is considered as an equative high-permeability porous medium (Pandey and Vishal, 2017). All the three layers are simplified to be uniform, isotropic and fully saturated with liquid water.

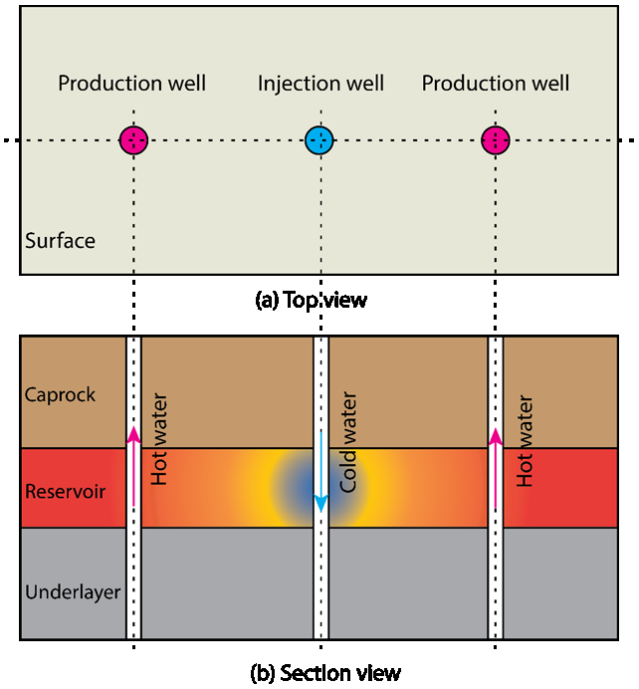

Figure 2: Schematic diagram of a typical EGS.

In this case study, the well distance in well pattern is 200 m. The distance from wellbore to lateral boundary is 100 m. Only a half of the model is established due to its symmetry about the injection-production-well section. A model with the cuboid dimensions of 400 ×100 ×100 m is established as shown in the Figure 3. The diameter of wellbore is 215.9 mm. The diameter and thickness of production casing are 139.7 and 9.17 mm, respectively.

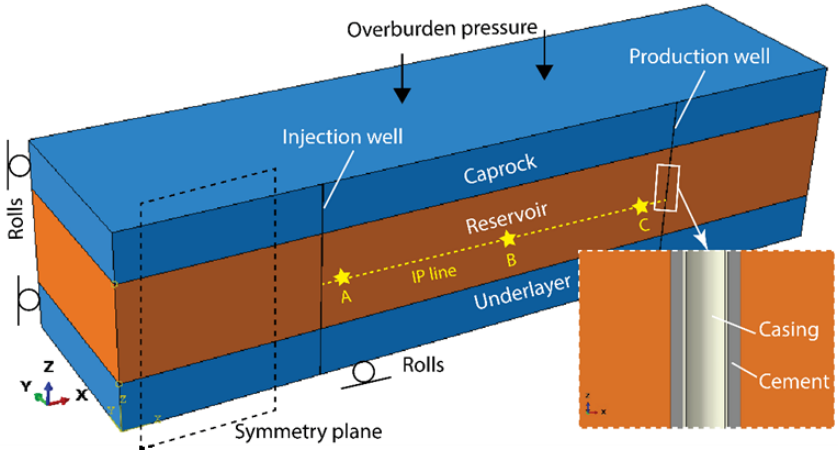

Figure 3: Model of reservoir and wells in EGS.

The IPW (injection-production wells) section of the model is constrained by symmetric condition. The top of the model is loaded by the overburden pressure. The other boundaries are constrained with rolls. The casing, cement sheath and wellbore are bonded together at the

cementing interfaces. The conventional hydrostatic and tensile loads of casing are not considered. The constant-pressure development is adopted, i.e., the excess pore pressures of injection well and production well are 5MPa and 0MPa, respectively. The temperature of injected water is 20℃. The initial temperature of the formation is 200℃. The gravity segregation and geothermal gradient in the reservoir are neglected. All the external boundaries are closed boundaries by setting it with no heat or flow fluxes across the external boundaries. The material properties of formation (Kim and Hosseini, 2015), cement and casing are listed in the Table 1.

Table 1: Material properties of formation, cement and casing.

Parameters (unit)	Value				
	Reservoir	Caprock /Underlayer	Water	Cement	Casing
Young's modulus (GPa)	30	30	-	7	210
Poisson's ratio (-)	0.25	0.25	-	0.23	0.3
Thermal conductivity (W/m/K)	3	3	0.58	2	52
Thermal expansion coefficient (K^{-1})	1.15e-6	1.15e-6	6.9e-5	1.0e-6	1.2e-5
Specific heat (J/kg/K)	1000	1000	4186	1000	434
Permeability (mD)	100	0.001	-	-	-
Porosity (-)	0.2	0.2	-	-	-
Density (kg/m^3)	2000	2000	1000	2500	7800

Abaqus was used to solve the coupled temperature–pore pressure-displacement element simultaneously by solving the temperature field as a nodal degree of freedom in addition to the displacement and the pore pressure fields.

2.3 Validation of Model

The solution of consolidation in saturated soil around a cylindrical heat source has been studied by Booker and Savvidou (1985). Numerical values for the parameters that define the geometry and the material properties are based on the works by Lewis and Schrefler and Abaqus guide (Abaqus). The proposed model is further simplified to a cubic soil with a cylindrical heat source in its center. The heat source is specified with a heat flux.

The profile of normalized temperature with normalized time is shown in Figure 4. In this figure, d and r represent the distance away from the center, and the radius of heat source, respectively. It indicates that the simulated results are consistent with the analytical results. Likewise, the simulated and analytical pore pressures are agreed. The comparison to analytical solution supplies a verification for the THM model.

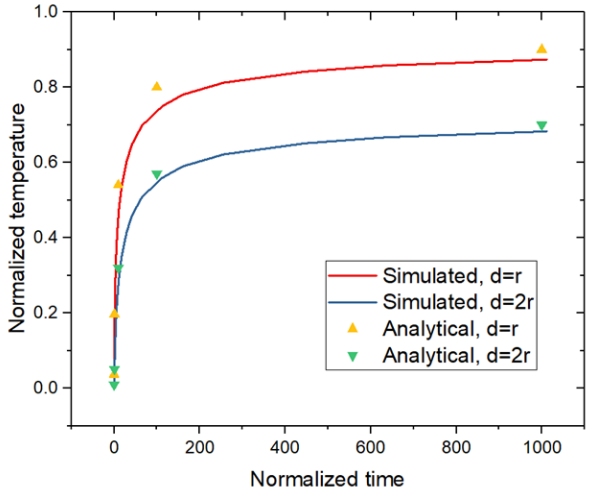

Figure 4: Variation of normalized temperature.

3. RESULTS AND DISCUSSION

By applying the proposed THM model of EGS, we conducted numerical simulation over a span of 20 years to investigate the spatial-temporal evolutions of poroelastic and thermal effects in porous medium together with the corresponding mechanical behavior of casing.

3.1 Evolutions of Temperature, Pressure and Stress

3.1.1 Pore Pressure

The line between the injection well and production well that lied in the half height of reservoir is captured to present the results. The distribution of excess pore pressure along the IP (injection-production) line at different time is shown in the Figure 5. The distance from injection well is normalized by the well distance (200 m), and he pore pressure is normalized by the injection pressure (5MPa). Water is injected at an excess pore pressure 5MPa, and the pore pressure in production well is kept as the initial hydrostatic pressure. The pore pressure decreases from injection well to production well. As time passes, the pore pressure in reservoir increases, while the increase rate decreases with time. The pore pressure distribution tends to be steady after one day.

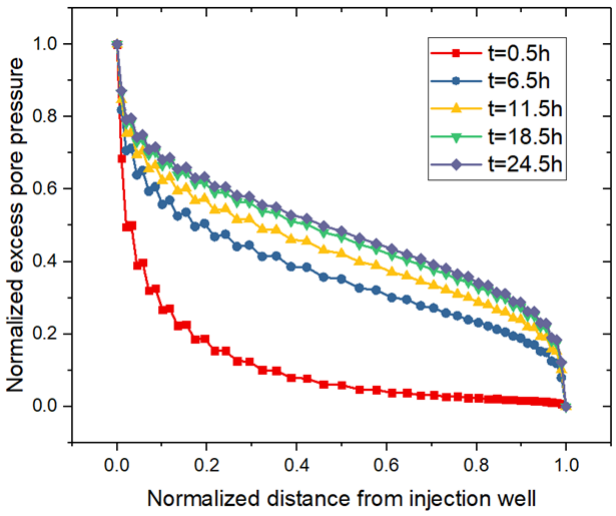

Figure 5: Distribution of excess pore pressure along the IP line at different time.

3.1.2 Temperature

The distribution of temperature drop along the IP line at different time is shown in the Figure 6. The temperature drop is normalized by the expression: TN= (T− Ti)/(Tw− Ti). In early period, the temperature around injection well decreases sharply, while the temperature around production well almost keeps the same value of initial temperature in reservoir. The water temperature rises when flowing through reservoir by heat transfer from rock. A relatively low-temperature region (LTR) forms around the injection well. As operation continues, the LTR expands gradually.

The evolution of temperature at one point of production wellbore with time is shown in Figure 7. It indicates that the temperature of the superheated water firstly keeps constant then decreases rapidly. The temperature decreases only 5℃ in the first decade, while it drops 69℃ in the following time. It is because that the heat transfer rate is decreasing with time due to the smaller and smaller temperature gradient. The cold front reached the production well after around 51 months and before that the production temperature is a constant. After thermal breakthrough, the decline rate of temperature at production well is large. By comparing with pore pressure variation, the propagation speed of temperature is much slower than that of overpressure along the IP line.

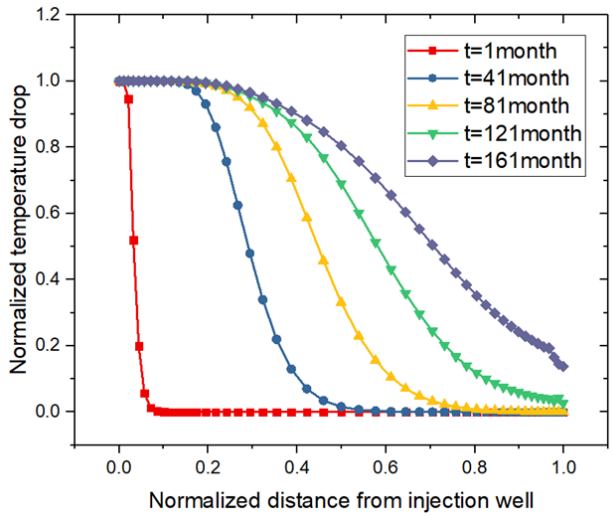

Figure 6: Distribution of temperature drop along the IP line at different time.

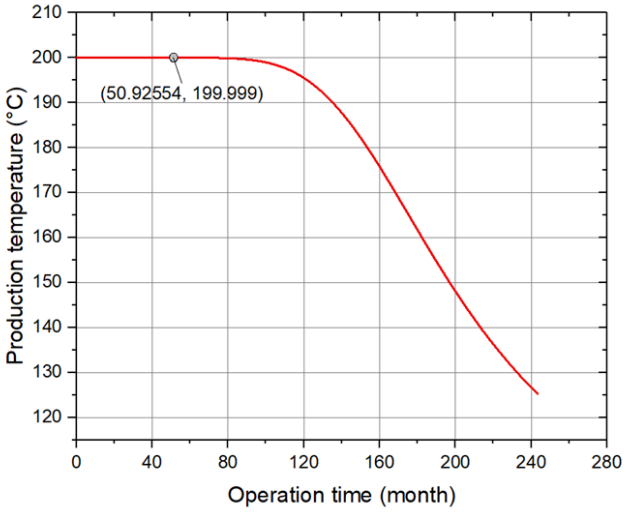

Figure 7: Evolution of temperature at production wellbore with time.

3.1.3 Stress/Deformation

The variations of pore pressure and temperature cause in-situ stress redistribution and deformation of reservoir. The distribution of radial stress change along the IP line at different time is shown in Figure 8. The stress change is normalized by the expression: SN=(S−Si)/Si. It demonstrates that the radial stress (similar with circumferential stress and vertical stresses) decreases around the injection well. According to the effective stress principle, overpressure can decrease the effective stress. Besides, temperature drop can cause rock contraction in LTR. The contraction effect can relax the compressive stress.

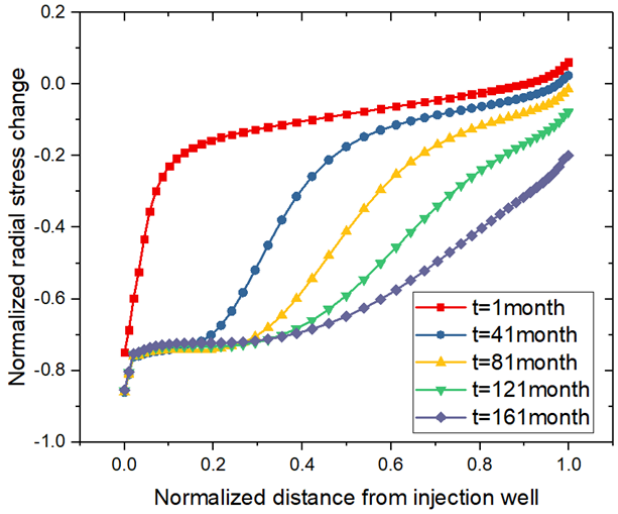

Figure 8: Distribution of radial stress along the IP line at different time.

The distribution of vertical displacement along the IP line at different time is shown in Figure 9. The stress change is normalized by the maximum displacement (4.336 mm). It indicates that the overpressure uplifts the formation in the early period. Whereas, the formation will subside as the thermal contraction expands. It can be inferred that the thermal effect overwhelms the poroelastic effect in the late period.

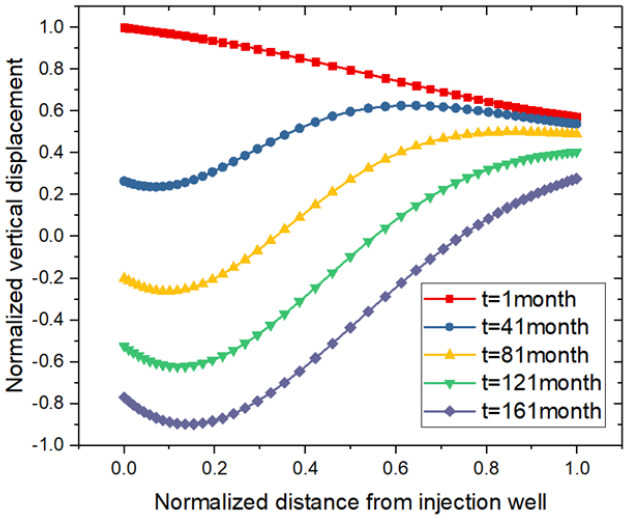

Figure 9: Distribution of vertical displacement along the IP line at different time.

The relationship among the normalized reservoir variables, including temperature, pore pressure, vertical stress and vertical displacement, as a function of location after 121 months are plotted in Figure 10. It demonstrates that the overpressure and cooling effects make the vertical effective stress decreasing wholly. The formation around the injection well subsides because the thermal contraction overwhelms the overpressure expansion. Whereas, the formation around the production well uplifts because the overpressure expansion exceeds the thermal contraction.

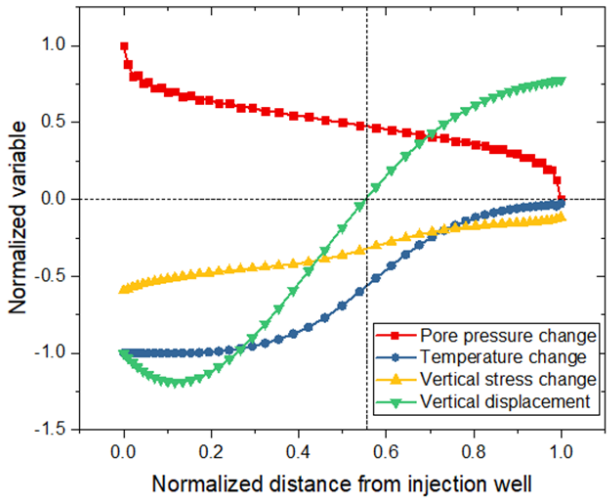

Figure 10: Relationship among the reservoir variables.

3.2 Casing Stress

The evolution of casing Mises stress in injection and production wells is shown in Figure 11. It indicates that the injection-production operation in EGS induces an additional stress on casing. The Mises stress of the casing in injection well is larger than that in production well within the span of 20 years. The Mises stress of the casing in injection well reaches to the maximum value after about 24 hours, because the pore pressure and temperature have almost completed the redistribution around the injection well in a short time. As the operation continues, the Mises stress of the casing in injection well decreases, while the Mises stress of the casing in production well increases gradually. It is caused by the rock thermal contraction after thermal breakthrough and casing thermal stress. Considering the long-time changing temperature and deformation in reservoir, we recommend that casing design should take the additional stress induced by the injection-production operation in EGS into account.

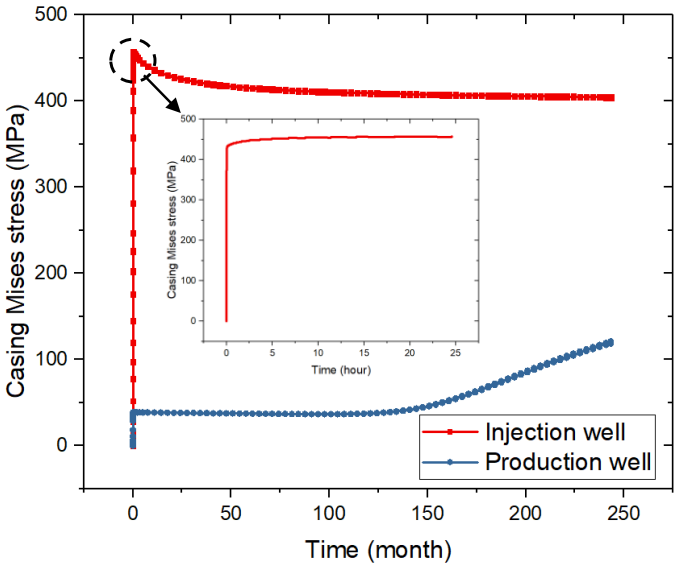

Figure 11: Evolution of casing Mises stress in injection and production wells.

4. CONCLUSIONS

A THM coupled model consisting of reservoir and well structure is established, which can be used to predict the spatial-temporal evolutions of the temperature, seepage and stress fields in EGS.

The pore pressure decreases from injection well to production well. The differential pressure drives water flowing towards production well. The water temperature rises during flowing and results in superheated water. A LTR forms around the injection well and expands as the operation continues. The cold front reached the production well after about 4.2 years. The decline rate of temperature at production well is large after thermal breakthrough. Temperature propagates much slower than overpressure.

The effective stress decreases around the injection well due to overpressure and thermal contraction. The low stress region (LSR) also expands with time. Overpressure uplifts the formation in the early period, whereas, formation subsides due to the expanding thermal contraction. The thermal effect overwhelms the poroelastic effect in late period.

The Mises stress of the casing in injection well reaches to the maximum value soon and then decreases slightly. While, the Mises stress of the casing in production well increases gradually after thermal breakthrough. Casing design should take this additional stress induced by the injection-production operation in EGS into account.

NOMENCLATURE

Symbol	Parameter
u	Displacement Vector
p	Pore Pressure
T	Temperature
λ, G	Lame Constant
α_B	Biot Coefficient
α_{Ts}	Thermal Expansion Coefficient of Rock Skeleton
f_i	Body Force Vector
$K_V = E/[3(1-2\nu)]$	Body Deformation Modulus
E	Young's Modulus
N	Poisson's Ratio.
K	Matrix of Permeability
m^{T}	[1 1 1 0 0 0]
ρ_w	Water Density
μ	Water Viscosity
ε	Volume Strain
ϕ	Porosity
α_{Tw}	Thermal Expansion Coefficient of Water
Q_m	Source Term.
$k_{heq} = k_{hw}\phi + k_{hs}(1-\phi)$	Equivalent Thermal Conductivity Coefficient
k_{hw}	Thermal Conductivity Coefficient of Water
k_{hs}	Thermal Conductivity Coefficient of Skeleton
$(\rho C)_{eq} = \rho_w C_w \phi + \rho_s C_s (1-\phi)$	Equivalent Specific Heat in Unit Volume
ρ_s	Density of Skeleton
C_w	Specific Heat of Water
C_s	Specific Heat of Skeleton
V_w	Flow Velocity
Q_h	Heat Flux
T	Temperature
T_i	Initial reservoir temperature
T_w	Injected water temperature
T_N	Normalized temperature
S	Effective stress
S_i	Initial effective stress
S_N	Normalized effective stress

REFERENCES

Aboustit, B.L., Advani, S.H. and Lee, J.K.: Variational Principles and Finite Element Simulations for Thermo-Elastic Consolidation, *International Journal for Numerical and Analytical Methods in Geomechanics*, **9(1)**, (1985), 49-69.

Booker, J.R. and Savvidou, C.: Consolidation Around a Point Heat Source, *International Journal for Numerical and Analytical Methods in Geomechanics*, **9(2)**, (1985), 173-184.

De Simone, S., Vilarrasa, V., Carrera, J., Alcolea, A. and Meier, P.: Thermal Coupling May Control Mechanical Stability of Geothermal Reservoirs During Cold Water Injection, *Physics and Chemistry of the Earth*, Parts A/B/C, **64**, (2013), 117-126.

Ge, J. and Ghassemi, A.: Analysis of Failure Potential Around a Hydraulic Fracture in Jointed Rock, 42nd US Rock Mechanics Symposium (USRMS), American Rock Mechanics Association, 2008.

Huang, X., Zhu, J., Li, J., Lan, C. and Jin, X.: Parametric Study of an Enhanced Geothermal System Based on Thermo-Hydro-Mechanical Modeling of a Prospective Site in Songliao Basin, *Applied Thermal Engineering*, **105**, (2016), 1-7.

Huang, X., Zhu, J., Niu, C., Li, J., Hu, X. and Jin, X.: Heat Extraction and Power Production Forecast of a Prospective Enhanced Geothermal System Site in Songliao Basin, China, *Energy*, **75**, (2014), 360-370.

Kim, S. and Hosseini, S.A.: Hydro-Thermo-Mechanical Analysis During Injection of Cold Fluid into a Geologic Formation, *International Journal of Rock Mechanics and Mining Sciences*, **77**, (2015), 220-236.

Lewis, R.W., Majorana, C.E. and Schrefler, B.A.: A Coupled Finite Element Model for the Consolidation of Nonisothermal Elastoplastic Porous Media, *Transport in Porous Media*, **1(2)**, (1986), 155-178.

Li, C. and Laloui, L.: Coupled Thermo-Hydro-Mechanical Effects on Caprock Stability During Carbon Dioxide Injection, *Energy Procedia*, **114**, (2017), 3202-3209.

Li, W., Soliman, M. and Han, Y.: Microscopic Numerical Modeling of Thermo-Hydro-Mechanical Mechanisms in Fluid Injection Process in Unconsolidated Formation, *Journal of Petroleum Science and Engineering*, **146**, (2016), 959-970.

Mossop, A.P.: Seismicity, Subsidence and Strain at the Geysers Geothermal Field, Ph.D. Thesis, Stanford University (2001).

Pandey, S.N., Chaudhuri, A. and Kelkar, S.: A Coupled Thermo-Hydro-Mechanical Modeling of Fracture Aperture Alteration and Reservoir Deformation During Heat Extraction from a Geothermal Reservoir, *Geothermics*, **65**, (2017), 17-31.

Pandey, S.N. and Vishal, V.: Sensitivity Analysis of Coupled Processes and Parameters on the Performance of Enhanced Geothermal Systems, *Scientific Reports*, **7(1)**, (2017), 17057.

Rawal, C.: 3D Modeling of Coupled Rock Deformation and Thermo-Poro-Mechanical Processes in Fractures, Ph.D. Dissertation, Texas A&M University, (2012).

Safari, R. and Ghassemi, A.: 3D Thermo-Poroelastic Analysis of Fracture Network Deformation and Induced Micro-Seismicity in Enhanced Geothermal Systems, *Geothermics*, **58**, (2015), 1-14.

Samsonov, S., Beavan, J., González, P.J., Tiampo, K. and Fernández, J.: Ground Deformation in the Taupo Volcanic Zone, New Zealand, Observed by ALOS PALSAR Interferometry, *Geophysical Journal International*, **187(1)**, (2011), 147-160.

Sarychikhina, O. and Glowacka, E.: Spatio-Temporal Evolution of Aseismic Ground Deformation in the Mexicali Valley (Baja California, Mexico) from 1993 To 2010, Using Differential SAR Interferometry, *Proceedings of the International Association of Hydrological Sciences*, **372**, (2015), 335.

Tao, H., Xie, K., Liu, G., Huang, D. and Deng, Y.: Finite Element Analysis of Foundation Consolidation by Vertical Drains Coupling Thermo-Hydro-Mechanical Effect, *Rock and Soil Mechanics*, **34(S1)**, (2013), 494-500.

Wang, K., Wu, X. and Liu, J.: Downhole Geothermal Power Generation in Oil and Gas Wells, GRC Transactions, 41, (2017).

White, J.A., Chiaramonte, L., Ezzedine, S., Foxall, W., Hao, Y., Ramirez, A., and McNab, W.: Geomechanical Behavior of the Reservoir and Caprock System at the In Salah CO2 Storage Project, *Proceedings,* National Academy of Sciences of the United States of America, **111(24)**, (2014), 8747-8752.

Ye, Z., Janis, M. and Ghassemi, A.: Injection-driven Shear Slip and the Coupled Permeability Evolution of Granite Fractures for EGS Stimulation, *Proceedings*, 51st US Rock Mechanics / Geomechanics Symposium, San Francisco, California, USA (2017).

Zhao, Y., Feng, Z., Feng, Z., Yang, D. and Liang, W.: THM (Thermo-Hydro-Mechanical) Coupled Mathematical Model of Fractured Media and Numerical Simulation of a 3D Enhanced Geothermal System at 573 K and Buried Depth 6000–7000 M, *Energy*, **82**, (2015), 193-205.